Data supplement for Shen et al., Subcortical Brain Development in Autism and Fragile X Syndrome: Evidence for Dynamic, Age- and Disorder-Specific Trajectories in Infancy. Am J Psychiatry (doi: 10.1176/appi.ajp.21090896)

SUPPLEMENTAL METHODS

Participants

Infants with FXS were enrolled and assessed at two clinical sites (University of North Carolina and Washington University). The presence of full mutation FXS was verified by medical records or genetic testing (PCR and Southern Blot). Infants at higher- and lower-likelihood for ASD were enrolled and assessed at four clinical sites (University of North Carolina, Washington University, University of Washington, and Children's Hospital of Philadelphia). Higher likelihood (HL) infants were defined by having an older sibling with a diagnosis of ASD made by their clinical provider, corroborated by meeting ASD classification on the Autism Diagnostic Interview-Revised (ADI-R) (1). Lower likelihood (LL) infants had a typically developing older sibling and no siblings with ASD at the time of enrollment (2).

All subjects were excluded for the presence of: (a) diagnosis or physical signs of known genetic conditions or syndromes other than FXS (e.g., significant dysmorphology, asymmetry on physical exam), significant medical or neurological conditions affecting growth, development or cognition (e.g., CNS infection, seizure disorder, diabetes, tuberous sclerosis, congenital heart disease) or sensory impairments such as significant vision or hearing loss, (or evidence of during the course of the study); (b) children with birth weight < 2000 grams and/or gestational age < 37 weeks, a history of significant perinatal adversity, exposure in-utero to neurotoxins (including alcohol, illicit drugs, selected prescription medications), or a history of maternal gestational diabetes; (c) contraindication for MRI (pacemaker, vascular stents, metallic ear tubes, other metal implants or braces); (d) families whose predominant home language is not English; and (e) children who are adopted. Parents provided informed consent, and the institutional review board at each site approved the research protocol.

Two LL infants that met criteria for ASD were excluded from the analysis because these were too few in number to constitute a comparison group and to maintain the family study design focused on ASD in the context of familial recurrence likelihood for ASD.

MRI Acquisition

Imaging data were collected at 6, 12, and 24 months for a total of 52 scans acquired in the FXS group, 167 in the HL-ASD group, 584 in the HL-neg group, and 296 in the LL-neg group (Supplemental Table 2). High-resolution T1- and T2-weighted imaging data ($1mm^3$ voxels) were acquired on 3T Siemens TIM Trio scanners with standard 12-channel head coils, and identical software versions. Scans with radiological abnormalities rated as clinically significant by a pediatric neuroradiologist (and confirmed by two independent pediatric neuroradiologists) were excluded (n=4). A description of the MRI acquisition, quality control, and reliability across acquisition sites are detailed in a previous publication on this sample (3).

Image Preprocessing

T1- and T2-weighted images underwent standard pre-processing (distortion correction, mutual registration, transformation to stereotactic space) and brain tissue segmentation. Specifically, all images were corrected for geometric distortions (4) and intensity non-uniformity (5). T2-weighted images underwent linear, rigid registration to the corresponding T1-weighted images via mutual information registration (6). Subsequently, both T1- and T2-weighted images were transformed to stereotactic space based on the registration of the T1 scan. The skull was extracted using a "majority voting approach" between the T1 atlas mask, T2 atlas mask, and the T1 and T2 images jointly (FSL Brain Extraction Tool) (7). All corrected and skull-stripped T1 and T2 images were used as input for an expectation, maximization-based, tissue segmentation tool (AutoSeg pipeline) to obtain white matter, gray matter, and CSF (8).

Segmentation of Subcortical Brain Structures

A graph-based, multi-atlas segmentation method developed by our laboratory (9) was employed to segment the subcortical structures with study- and age-specific multi-atlas template sets, as previously described (10). First, all atlases and participant MR images were paired and co-registered via symmetric diffeomorphic registration using the ANTS (Advanced

Normalization ToolS) registration tool (11). Second, a directed graph with edge weights based on intensity and shape similarity was constructed between all atlases and the participant MR image (9). Third, the shortest path from each atlas to the participant image was computed (with atlases sharing the same shortest paths combined into the same cluster), and the atlas closest to the participant for each cluster was selected as the neighboring template (9). Lastly, the final segmentation was produced by fusing the propagated label files of the neighboring templates via weighted majority voting (9). The caudate segmentations were additionally refined by using the separately segmented lateral ventricles as a mask (12). Atlas templates were derived from 8 infant MRI cases at each time point (6, 12, and 24 months), which were manually segmented by a single experimenter. In order to eliminate any template induced asymmetric laterality biases, we employed left-right flipped versions of all atlas images in the multi atlas segmentation, resulting in a total of 16 atlas templates at each timepoint, or 48 atlas images in total. These were used as training images in the multi atlas segmentation, and then applied to all 6 month and 12-24 month data sets. The multi-atlas segmentation method was validated in a leave-one-out validation analysis that achieved high Dice coefficients for all structures (mean=91.47%, SD=.03, range=87.20-96.00%). All segmentations underwent visual quality inspection by two experimenters (blind to diagnosis, familial likelihood status, sex, scan site). Ninety-eight percent of scans met quality inspection criteria for inclusion in the final analysis (N=1099 scans; Supplemental Table 2).

The laterality of each structure was thoroughly evaluated in a previous publication on this sample to determine if left and right subcortical volumes should be treated separately, or summed together (10). To assess potential hemispheric differences, a Laterality Index (LI) was created according to the published formula (13): LI = 1 * (Left-Right)/(Left+Right). This formula results in values ranging from -1 to +1, and a common threshold for hemispheric dominance is over 0.2 (14). The sign of LI indicates the direction of asymmetry, with positive values indicating larger left side volumes, and negative values indicating larger right side volumes. As reported in (10), LI values for each subcortical structure were all virtually 0, and no individual in the study exceeded 0.08, far less than the threshold for hemispheric dominance of 0.2 (14). Given the lack of laterality, and as there were no group-by-laterality interactions observed in any subcortical structure, the left and right volume were summed and analyzed as a total volume of each structure (10).

The complete Autoseg software pipeline for multi-atlas-based segmentation is publicly available on the NIH NITRC website (Neuroimaging Informatics Tools and Resources Clearinghouse) at http://www.nitrc.org/projects/autoseg. Data management was provided by the IBIS Data Coordinating Center at the Montreal Neurological Institute (15). Supplemental Figure 1 shows the results of the segmentation of left and right caudate, amygdala, thalamus, putamen, and globus pallidus.

Statistical Analysis

A longitudinal mixed effects model for repeated measures with unstructured covariance matrices was employed to analyze trajectories of subcortical structures from 6 to 24 months of age. This analytic method is suitable for an unbalanced design and allows for missing values in a longitudinal study. Independent variables of interest included main effect of group, linear effect of age, sex, and group interactions with each of these variables. Total cerebral volume (TCV) was included as a covariate given its relationship to subcortical volumes and to control for brain size. Scan site was included as another control variable. Following significant omnibus results of the primary model described above, pairwise comparisons tested for cross-sectional group differences at each time point (6, 12 and 24 months) and were corrected for multiple comparisons (Tukey-Kramer). Percent differences in model-adjusted volumes at each time point and Cohen's *d* effect sizes are reported relative to the LL-negative group. In the ASD group, linear regression was used to test whether amygdala volume growth rate between 6-12 months was associated with social deficits at 24 months (ADOS Social Affect calibrated severity score), or alternatively with restricted and repetitive behaviors at 24 months (ADOS Restricted, Repetitive Behaviors calibrated severity score and the RBS-R overall score), which calibrate the severity scores for the two domains across ADOS modules and versions, making the scores comparable (16–18). The formula for amygdala volume growth rate measures the percent change in amygdala volume between two time points, normalized by the exact age interval between the time points. For example, the percentage change between the scans at 6 and 12 months is normalized by a correction factor that approaches 1 when the age interval between the scans is exactly 6 months: $((\text{Amygdala}_{12\text{ months}} - \text{Amygdala}_{6\text{ months}}) / \text{Amygdala}_{6\text{ months}})) * 100 * (6 / (\text{Age}_{12\text{months}} - \text{Age}_{6\text{months}}))$. This brain-behavior analysis was restricted to those subjects who had the required imaging data at both 6 and 12 months and behavioral data at 24 months. In the FXS

group, linear regression was used to test whether caudate volume at 12 months (the time point with the highest number of FXS scans) was associated with the repetitive behaviors at 24 months (RBS-R overall score). This analysis was restricted to those subjects who had the required imaging data at 12 months and behavioral data at 24 months. All tests were two-tailed with $\alpha = 0.05$, corrected. All analyses were performed using SAS JMP software (SAS Institute, Cary, NC). There was no site by group interaction, site by age interaction, or main effect of site on amygdala or caudate volumes. There were significant positive relationships between amygdala and caudate volumes, similarly in FXS and ASD at 6 months (r=.51; r=.64; respectively), and at 12 months (r=.57; r=.51).

REFERENCES

1. Lord C, Rutter M, Couteur A: Autism Diagnostic Interview-Revised: A revised version of a diagnostic interview for caregivers of individuals with possible pervasive developmental disorders. Journal of Autism and Developmental Disorders 1994; 24:659–685

2. Estes A, Zwaigenbaum L, Gu H, et al.: Behavioral, cognitive, and adaptive development in infants with autism spectrum disorder in the first 2 years of life. J Neurodev Disord 2015; 7:24

3. Hazlett HC, Gu H, McKinstry RC, et al.: Brain volume findings in 6-month-old infants at high familial risk for autism. The American journal of psychiatry 2012; 169:601–608

4. Fonov VS, Janke A, Caramanos Z, et al.: Improved Precision in the Measurement of Longitudinal Global and Regional Volumetric Changes via a Novel MRI Gradient Distortion Characterization and Correction Technique. Medical Imaging and Augmented Reality 2010; 6326:324–333

5. Sled JG, Zijdenbos AP, Evans AC: A nonparametric method for automatic correction of intensity nonuniformity in MRI data. IEEE Trans Med Imaging 1998; 17:87–97

6. Collins DL, Neelin P, Peters TM, et al.: Automatic 3D Intersubject Registration of MR Volumetric Data in Standardized Talairach Space. Journal of Computer Assisted Tomography 1994; 18:192

7. Smith SM: Fast robust automated brain extraction. Hum Brain Mapp 2002; 17:143–155

8. Gouttard S, Styner M, Joshi S, et al.: Subcortical structure segmentation using probabilistic atlas priors. SPIE Medical Imaging Image Processing Proceedings 2007; 6512:88

9. Wang J, Vachet C, Rumple A, et al.: Multi-atlas segmentation of subcortical brain structures via the AutoSeg software pipeline. Frontiers in neuroinformatics 2014; 8:7

10. Swanson MR, Shen MD, Wolff JJ, et al.: Subcortical Brain and Behavior Phenotypes Differentiate Infants With Autism Versus Language Delay. Biological Psychiatry: Cognitive Neuroscience and Neuroimaging 2017; 2:664–672

11. Avants BB, Epstein CL, Grossman M, et al.: Symmetric diffeomorphic image registration with cross-correlation: evaluating automated labeling of elderly and neurodegenerative brain. Med Image Anal 2008; 12:26–41

12. Shen MD, Kim SH, McKinstry RC, et al.: Increased Extra-axial Cerebrospinal Fluid in High-Risk Infants who Later Develop Autism. Biological Psychiatry 2017; 82:186–193

13. Seghier ML: Laterality index in functional MRI: methodological issues☆. Magn Reson Imaging 2008; 26:594–601

14. Springer JA, Binder JR, Hammeke TA, et al.: Language dominance in neurologically normal and epilepsy subjects: a functional MRI study. Brain J Neurology 1999; 122 (Pt 11):2033–46

15. Das S, Glatard T, MacIntyre LC, et al.: The MNI data-sharing and processing ecosystem. Neuroimage 2016; 124:1188–1195

16. Gotham K, Pickles A, Lord C: Standardizing ADOS scores for a measure of severity in autism spectrum disorders. Journal of Autism and Developmental Disorders 2009; 39:693–705

17. Gotham K, Risi S, Pickles A, et al.: The Autism Diagnostic Observation Schedule: revised algorithms for improved diagnostic validity. Journal of Autism and Developmental Disorders 2007; 37:613–627

18. Gotham K, Pickles A, Lord C: Trajectories of Autism Severity in Children Using Standardized ADOS Scores. PEDIATRICS 2012; 130:e1278-84

TABLE S1. Participant characteristics by group

	Mean (SD)				
	FXS	**HL-ASD**	**HL-Negative**	**LL-Negative**	**p-value**
N	29	58	212	109	
Sex	23 M; 6 F	46 M; 12 F	119 M; 93 F	66 M; 43 F	<.0001
Age at 1st MRI (mo.)	6.8 (1.0)	6.6 (.7)	6.7 (.7)	6.7 (.6)	ns
Age at 2nd MRI (mo.)	12.6 (.8)	12.7 (.7)	12.7 (.7)	12.7 (.7)	ns
Age at 3rd MRI (mo.)	24.5 (.8)	24.7 (1.1)	24.8 (1.0)	24.8 (.9)	ns
Mullen Early Learning Composite (at 24 mos.)	61.4 (14.1)	81.4 (17.1)	103.4 (15.8)	110.5 (16.1)	<.0001

Note: p-value of Chi-square test (sex) and omnibus ANOVA (Age, Mullen)

TABLE S2. Number of MRI scans at each time point

	Number of MRIs			
	6 months	**12 months**	**24 months**	**TOTAL**
Fragile X	**17**	**23**	**12**	**52**
HL-ASD	**57**	**52**	**58**	**167**
HL-Negative	**182**	**212**	**190**	**584**
LL-Negative	**109**	**105**	**82**	**296**
TOTAL	**365**	**392**	**342**	**1099**

FIGURE S1. Segmentation of subcortical brain structures. (A) T1-weighted coronal image of an infant with fragile X at 12 months of age. (B) 3-dimensional volumetric rendering of subcortical segmentations. *(Red: amygdala; Green: caudate; Cyan: putamen; Yellow: globus pallidus; Pink: thalamus.)*

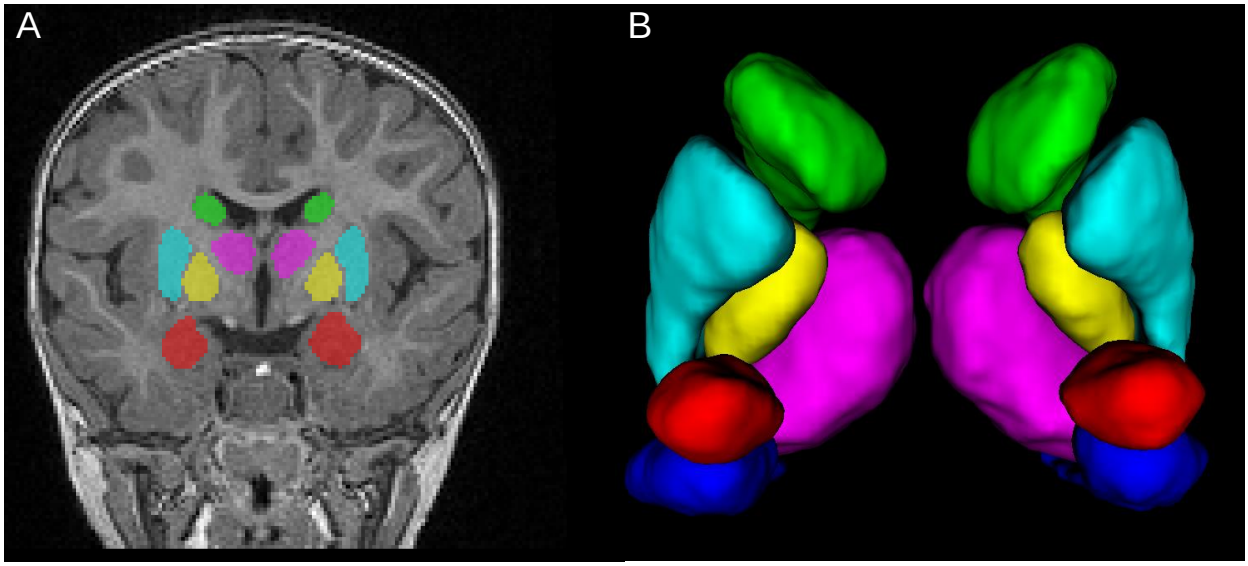

FIGURE S2. Infants with fragile X had larger globus pallidus volumes

*Note: Significant main effect of group (p<.0001). ***p<.0001 (corrected) vs. all other groups. **p<.005 (corrected) vs. all other groups. Plots of the model-adjusted LS means (error bars = ±1 SEM) are overlaid onto the raw data points of all participants. Percent differences in LS means are in relation to the LL-negative group. (Note that the lines for the LL-negative (blue) and HL-negative (purple) lines are overlapping.)*

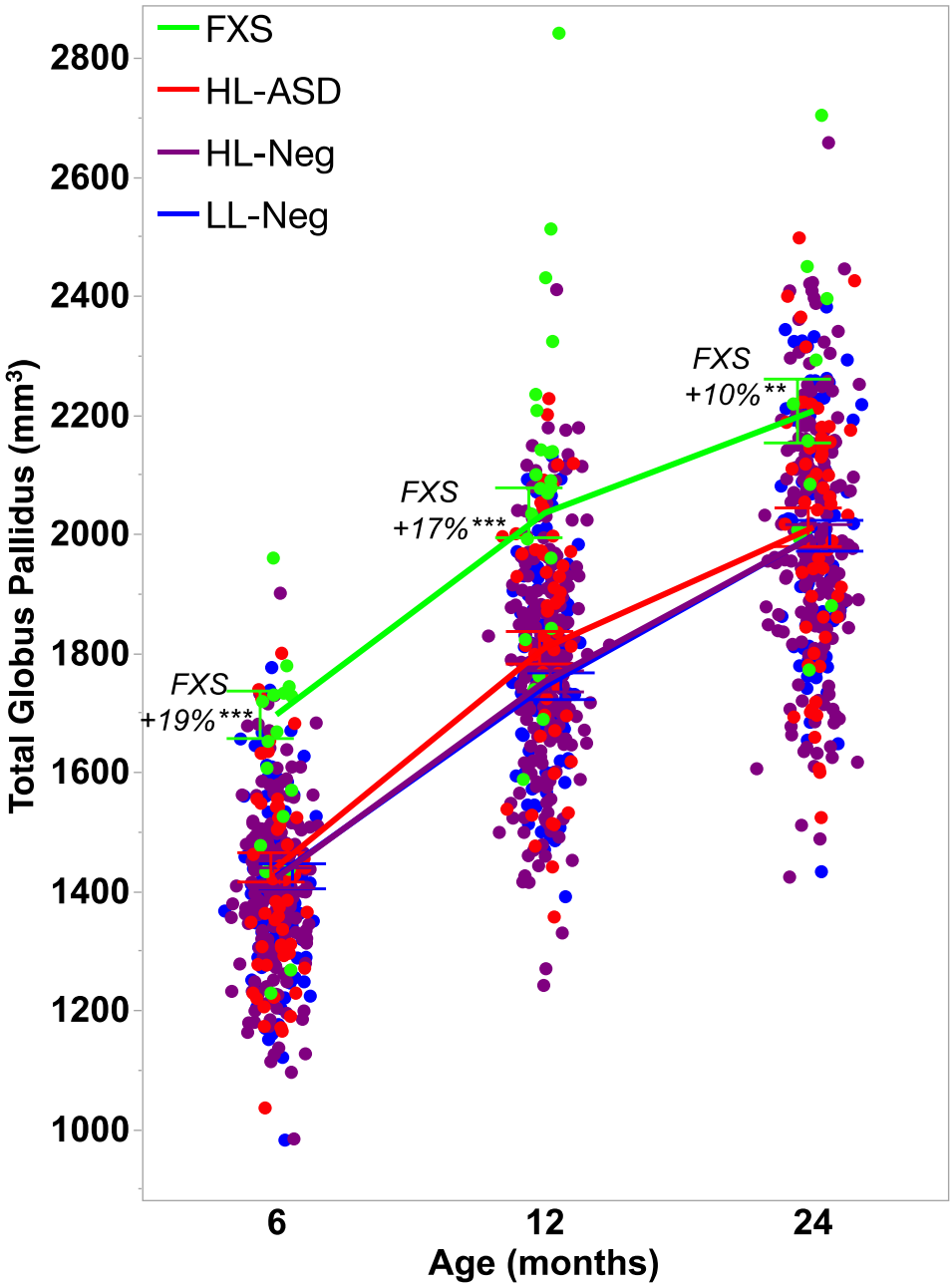

FIGURE S3. Infants with fragile X had larger putamen volumes

*Note: Significant main effect of group (p<.0001). **p<.005 (corrected) vs. all other groups. Plots of the model-adjusted LS means (error bars = ±1 SEM) are overlaid onto the raw data points of all participants. Percent differences in LS means are in relation to the LL-negative group.*

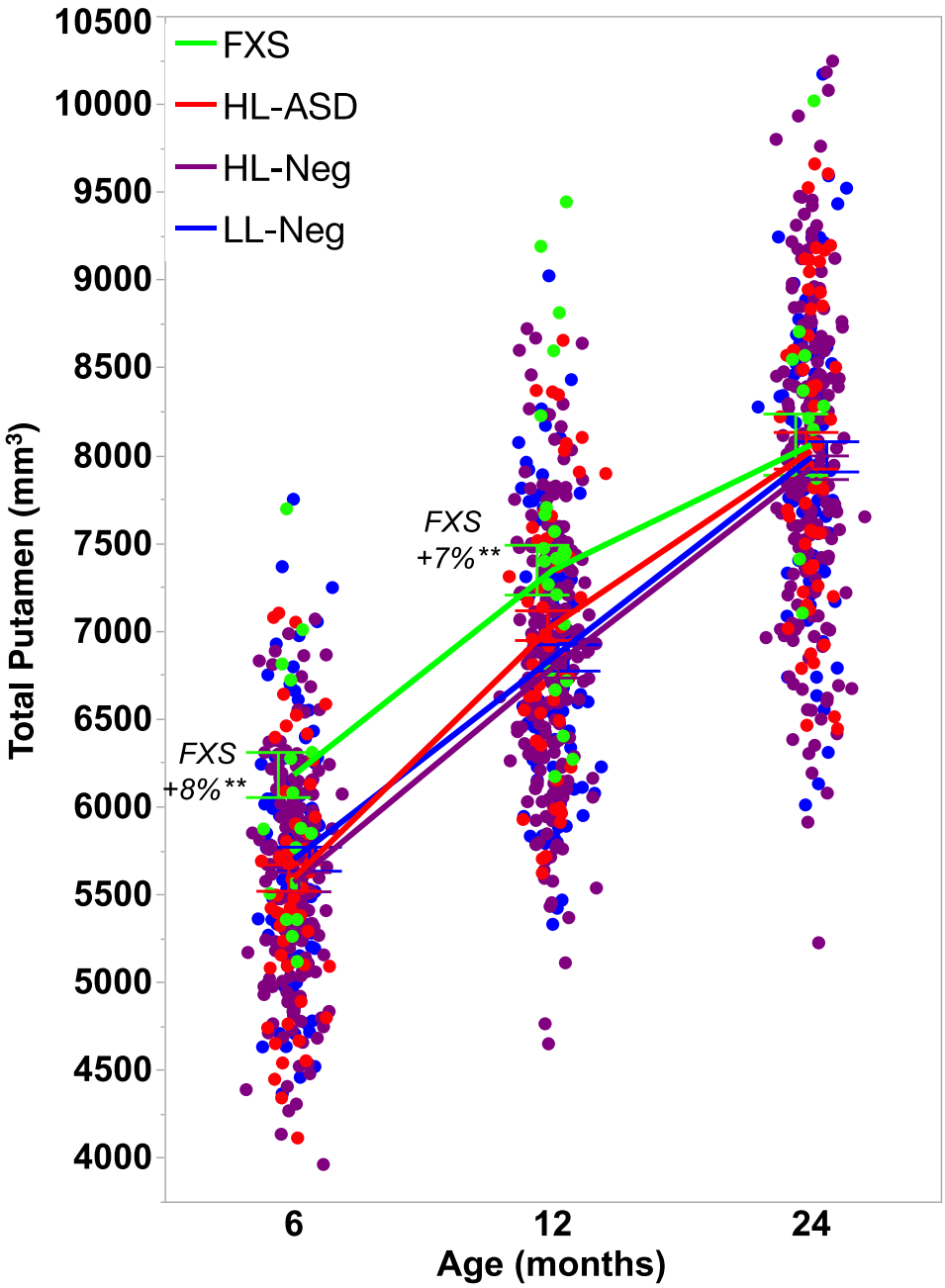

FIGURE S4. No group differences in thalamus volumes

Note: Non-significant main effect of group (p=.30). Plots of the model-adjusted LS means (error bars = ±1 SEM) are overlaid onto the raw data points of all participants.